1 **Title Page**

2

3 **A Drug-Tunable Flt23k Gene Therapy for Controlled Intervention in Retinal**
4 **Neovascularization**

5

6 Jinying Chen[1,2], Fan-Li Lin[2,3], Jacqueline Y.K. Leung[4], Leilei Tu[1], Jiang-Hui Wang[5], Yu-Fan
7 Chuang[2,4], Fan Li[2,6], Hsin-Hui Shen[7,8], Gregory J. Dusting[5,9], Vickie H.Y. Wong[10], Leszek
8 Lisowski[11,12,13], Alex W. Hewitt[2,5,9], Bang V. Bui[10], Jingxiang Zhong[1,14], Guei-Sheung Liu[1,2,9,14*]

9

10 [1]Department of Ophthalmology, the First Affiliated Hospital of Jinan University, Guangzhou, China

11 [2]Menzies Institute for Medical Research, University of Tasmania, Hobart, Australia

12 [3]Shenzhen Key Laboratory of Biomimetic Materials and Cellular Immunomodulation, Shenzhen
13 Institute of Advanced Technology, Chinese Academy of Sciences, Shenzhen, China

14 [4]Wicking Dementia Research and Education Centre, University of Tasmania, Hobart, Australia

15 [5]Centre for Eye Research Australia, Royal Victorian Eye and Ear Hospital, East Melbourne, Australia

16 [6]State Key Laboratory of Ophthalmology, Zhongshan Ophthalmic Centre, Sun Yat-sen University,
17 Guangzhou, China

18 [7]Department of Materials Science and Engineering, Faculty of Engineering, Monash University,
19 Clayton, Australia

20 [8]Department of Biochemistry and Molecular Biology, School of Biomedical Science, Monash
21 University, Clayton, Australia

22 [9]Ophthalmology, Department of Surgery, University of Melbourne, East Melbourne, Australia

23 [10]Department of Optometry and Vision Sciences, University of Melbourne, Parkville, Australia

24 [11]Translational Vectorology Group, Children's Medical Research Institute, Faculty of Medicine and
25 Health, University of Sydney, Sydney, Australia

26 [12]Vector and Genome Engineering Facility, Children's Medical Research Institute, Faculty of
27 Medicine and Health, University of Sydney, Sydney, Australia

28 [13]Military Institute of Hygiene and Epidemiology, The Biological Threats Identification and
29 Countermeasure Centre, 24-100 Puławy, Poland

30 [14]JZ and GSL contributed equally to this work as senior author.

31

32 *Correspondence and requests for materials should be addressed to Dr Guei-Sheung Liu
33 (rickliu0817@gmail.com). Menzies Institute for Medical Research, University of Tasmania. Address:
34 17 Liverpool Street, Hobart, TAS 7000, Australia. Tel: +61362264250.

35

36 Running title: Tunable gene therapy for retinal neovascularization

Abstract

Gene therapies that chronically suppress vascular endothelial growth factor (VEGF) represent a new approach for managing retinal vascular leakage and neovascularization. However, constitutive suppression of VEGF in the eye may have deleterious side effects. Here, we developed a novel strategy to introduce Flt23k, an intraceptor that binds intracellular VEGF, fused to the destabilizing domain (DD) of *Escherichia coli* dihydrofolate reductase (DHFR) into the retina. The expressed DHFR(DD)-Flt23k fusion protein is degraded unless "switched on" by administering a stabilizer; in this case, the antibiotic trimethoprim (TMP). Cells transfected with the DHFR(DD)-Flt23k construct expressed the fusion protein at levels correlated with the TMP dose. Stabilization of the DHFR(DD)-Flt23k fusion protein by TMP was able to inhibit intracellular VEGF in hypoxic cells. Intravitreal injection of self-complementary adeno-associated viral vector (scAAV)-DHFR(DD)-Flt23k and subsequent administration of TMP resulted in tunable suppression of ischemia-induced retinal neovascularization in a rat model of oxygen-induced retinopathy (OIR). Hence, our study suggests a promising novel approach for the treatment of retinal neovascularization.

Introduction

Retinal neovascularization is a key pathological feature of several leading causes of vision loss, including diabetic retinopathy, retinopathy of prematurity, and retinal vein occlusions[1]. In these diseases, abnormally high levels of vascular endothelial growth factor (VEGF) have been observed in the retina. Excessively high levels of VEGF cause pathological vascular leakage and the formation of new blood vessels in the retina, which can lead to vision loss. Intraocular injections of anti-VEGF agents (such as VEGF-neutralizing proteins) have been shown to reduce blood vessel leakage, allowing fluid reabsorption and resulting in improved visual acuity[2]. However, as this approach does not address the cause of VEGF production, leakage and neovascularization will recur when the vitreous levels of exogenous anti-VEGF proteins drop below therapeutic levels. Thus, current regimens require frequent (as often as monthly) and prolonged treatment, sometimes for many years, to maintain visual acuity[3]. Although intraocular delivery of anti-VEGF agents is generally safe, some of the drugs administered can enter the systemic circulation, where chronically high levels of anti-VEGF proteins can increase the risk of systemic adverse effects[4].

Recently, the utilization of gene therapies with the potential to chronically suppress the production of VEGF in the retina has been proposed as an attractive way to manage ocular neovascularization[5,6]. While promising, chronic VEGF suppression may have deleterious side effects on the retina. As the disease course can fluctuate between periods of relative VEGF inactivity and high activity in many patients, a gene therapy approach that can accommodate such fluctuations during the course of disease would potentially be a safer and more effective approach than an approach with prolonged VEGF suppression. In this study, we created a fusion gene consisting of an intracellular VEGF-targeting decoy receptor, Flt23k[7], and a protein disruption system (based on the destabilizing domain (DD) of *Escherichia coli* dihydrofolate reductase (DHFR); DHFR (DD)-Flt23k)[8,9]. Flt23k consists of domains 2-3 of VEGF receptor 1 (VEGFR1, the highest-affinity VEGF receptor) coupled to the C-terminal endoplasmic reticulum (ER) retention signal KDEL, a tetrapeptide (Lys-Asp-Glu-

Leu). Flt23k binds intracellular VEGF and sequesters it in the ER, where VEGF undergoes proteasomal degradation[10,11]. Without a triggering molecule, the expressed DHFR(DD)-Flt23k fusion protein becomes unfolded and ubiquitinated and then is rapidly processed by the proteasome, resulting in degradation of the entire fusion protein[12]. A stabilizing drug such as the antibiotic trimethoprim (TMP) reliably prevents proteasomal destruction of DHFR(DD)-Flt23k, which then binds to intracellular VEGF and prevents VEGF secretion (**Figure 1a**, illustration). In addition, to achieve long-term and early-onset gene expression, a self-complementary adeno-associated viral vector (scAAV)[13] was utilized to deliver the DHFR(DD)-Flt23k gene into the back of the eye via a single intravitreal injection. Our data demonstrated that gene delivery of *DHFR(DD)-Flt23k* and subsequent administration of TMP allowed disruption of VEGF levels *in vitro*. Importantly, we also showed that this approach resulted in tunable suppression of retinal neovascularization in a rat model of oxygen-induced retinopathy (OIR).

Results

Design and validation of the DHFR-based destabilized domain approach *in vitro*.

scAAVs encoding enhanced green fluorescent protein (EGFP) (or mCherry), Flt23k, DHFR(DD)-yellow fluorescent protein (YFP) (or DHFR(DD)-mCherry), DHFR(DD)-Flt23k, or Flt23k-DHFR(DD) were designed and constructed for the study (**Figure 1b**). We first validated whether the DHFR(DD)-protein destabilizing system could be controlled using the stabilizing ligand TMP *in vitro*. Human embryonic kidney 293A (HEK293A) cells were transfected with scAAV plasmid (pscAAV)-mCherry, pscAAV-Flt23k, pscAAV-DHFR(DD)-YFP, pscAAV-DHFR(DD)-Flt23k or pscAAV-Flt23k-DHFR(DD) for 24 hours and then exposed to 10 μM TMP or varying doses of TMP (0, 2, 10, and 50 μM) for 24 hours. A 42-kDa band for DHFR(DD)-Flt23k or Flt23k-DHFR(DD) or a 25-kDa Flt23k protein was detectable in pscAAV-DHFR(DD)-Flt23k, pscAAV-Flt23k-DHFR(DD) and

pscAAV-Flt23k-transfected cells, respectively, by western blotting. Neither protein was found in pscAAV-DHFR(DD)-YFP- or pscAAV-mCherry-transfected cells (**Figure 1c**). Compared with the construct with C-terminal fusion of Flt23k (Flt23k-DHFR(DD): 1.41-fold increase, p<0.05; n=3), the construct with N-terminal fusion (DHFR(DD)-Flt23k: 2.66-fold increase, p<0.001; n=3) was more flexibly regulated by TMP, as evidenced by relatively low DHFR(DD)-Flt23k protein levels in the absence of TMP and high levels following TMP exposure (**Figure 1d**). Interestingly, we observed a slight increase in DHFR(DD)-Flt23k expression in pscAAV-DHFR(DD)-Flt23k-transfected cells even without TMP, indicating that some undegraded proteins remained despite the DHFR(DD)-protein destabilizing system.

Next, we investigated whether DHFR(DD)-Flt23k is dependent on the TMP dose *in vitro*. Compared to no TMP, the addition of 2, 10 or 50 μM TMP to the culture medium resulted in an increase in cytosolic DHFR(DD)-Flt23k expression (2 μM: 2.12-fold, 10 μM: 3.14-fold, 50 μM: 4.45-fold; p<0.05, n=4) (**Figure 1e and 1f**). Although DHFR(DD)-Flt23k protein levels rose with increasing doses of TMP, no significant difference was found between 10 and 50 μM TMP treatment (p=0.2330). These data suggest that the N-terminal fusion construct DHFR(DD)-Flt23k is more flexibly regulated and can be dose-dependently stabilized by TMP.

Stabilization of DHFR(DD)-Flt23k functionally inhibits hypoxia-induced VEGF *in vitro*.

Next, we considered whether the product resulting from TMP induction of DHFR(DD)-Flt23k was biologically active by examining its capacity to inhibit hypoxia-induced human VEGF production. HEK293A cells were transfected with pscAAV-DHFR(DD)-Flt23k for 24 hours and exposed to TMP at a dose between 0 and 50 μM for 24 hours. The cells were incubated under hypoxic conditions for 24 hours. Cell lysates and conditioned medium were harvested for enzyme-linked immunosorbent assay (ELISA)-based detection of VEGF. Under the hypoxic conditions, compared to pscAAV-mCherry-transfected cells, the cells transduced with pscAAV-Flt23k (intracellular VEGF: 190 ± 27

126   pg/μg, p<0.05, n=6-7; extracellular VEGF: 1156 ± 107 pg/mL, p<0.05, n=7) showed reductions in

127   both intracellular and extracellular VEGF levels (intracellular VEGF: 315 ± 32 pg/μg; extracellular

128   VEGF: 1564 ± 102 pg/mL; n=5) (**Figure 2a and 2b**). Cells transfected with pscAAV-DHFR(DD)-

129   Flt23k showed a significant decrease in the intracellular VEGF concentration, an effect that was

130   dependent on the dose of TMP (DHFR(DD)-Flt23k: 198 ± 19 pg/μg; DHFR(DD)-Flt23k with 2 μM

131   TMP: 95 ± 16 pg/μg; DHFR(DD)-Flt23k with 10 μM TMP: 63 ± 13 pg/μg, p<0.05; DHFR(DD)-Flt23k

132   with 50 μM TMP: 45 ± 14 pg/μg, p<0.01; n=8) (**Figure 2a**). Similarly, the cells transfected with

133   pscAAV-DHFR(DD)-Flt23k also showed a significant TMP-dependent decrease in extracellular

134   VEGF secretion (DHFR(DD)-Flt23k: 1192 ± 79 pg/mL; DHFR(DD)-Flt23k with 2 μM TMP: 828 ±

135   89 pg/mL; DHFR(DD)-Flt23k with 10 μM TMP: 601 ± 97 pg/mL, p<0.01; DHFR(DD)-Flt23k with

136   50 μM TMP: 507 ± 92 pg/mL, p<0.001; n=7) (**Figure 2b**). Together, our *in vitro* data suggest that

137   gene delivery of DHFR(DD)-Flt23k can reduce the VEGF protein level in a TMP-controlled manner.

138   Interestingly, we also found that cells transfected with pscAAV-DHFR(DD)-YFP (intracellular

139   VEGF: 388 ± 33 pg/μg, n=7; extracellular VEGF: 1544 ± 92 pg/mL, n=8) showed a significant

140   decrease in intracellular (153 ± 24 pg/μg, p<0.001, n=8) and extracellular (932 ± 113 pg/mL, p<0.01,

141   n=7) VEGF levels when exposed to 50 μM TMP (**Figure 2a**). We investigated whether the high dose

142   of TMP inhibits VEGF expression using quantitative polymerase chain reaction (qPCR). Under

143   hypoxic conditions, cells were exposed to TMP at a dose between 0.01 and 100 μM, and compared to

144   no TMP, the high dose of TMP (100 μM) decreased VEGF gene expression (**Figure S1a**). We then

145   confirmed that compared to cells not treated with TMP, cells transfected with pscAAV-DHFR(DD)-

146   YFP (fold change in *VEGFA* mRNA: 8.1 ± 0.7, p<0.05; n=3) or pscAAV-DHFR(DD)-Flt23k (fold

147   change in *VEGFA* mRNA: 7.8 ± 0.4, p<0.05; n=3) and then exposed to 50 μM TMP also showed a

148   decrease in VEGF gene expression (DHFR(DD)-YFP: 17.2 ± 1.9; DHFR(DD)-Flt23k: 15.0 ± 1.6; n=3)

149   (**Figure S1b**). Thus, our results indicate that a high dose of TMP (> 10 μM) may also inhibit VEGF

150   gene expression.

151

Efficiency of scAAV2-mediated gene delivery and validation of transgene product regulation by the DHFR(DD)-protein destabilizing system in rat retinas.

The rat OIR model was employed to evaluate the therapeutic potential of drug-tunable Flt23k gene therapy in retinal neovascularization. We first assessed the effectiveness of scAAV2-mediated gene delivery in OIR rats. Eleven days after intravitreal injection of scAAV2-EGFP into OIR rats (postnatal day 18 [P18]), EGFP expression was evident across the whole flat-mount retina (**Figure 3a**). Retinal cross-sections also showed that scAAV2 drove strong panretinal expression across all retinal layers (including the ganglion cell layer, inner nuclear layer and outer nuclear layer), as evidenced by the presence of EGFP (**Figure 3b**). Given that retinal glia are a potential cellular source of VEGF, we further characterized scAAV2-mediated transgene expression in retinal glial cells using colabeling of glial fibrillary acidic protein (GFAP; a marker of glial cells). We found that scAAV2 was able to drive gene expression in GFAP-positive retinal glial cells (**Figure 3c**).

To verify the hypothesis that DHFR(DD) provides control of the expressed fusion protein *in vivo*, P7 rat pups were intravitreally injected with scAAV2-DHFR(DD)-YFP and then received an intraperitoneal injection of 3 µg TMP on P14 and P16. Eyes were harvested on P18 to validate the expression of DHFR(DD)-YFP (**Figure 3d**). We found that a few YFP fluorescence-positive cells were present without TMP treatment but YFP protein levels were significantly elevated after the stabilization of DHFR(DD)-YFP by systemic injection of TMP (**Figures 3e and S2**). A similar pattern indicating a drug-tunable effect was shown in scAAV2-DHFR(DD)-mCherry-treated retinas of OIR rats (**Figure S3**). To further verify that the drug-tunable effect of the DHFR(DD)-fusion protein is mediated through posttranslational regulation, DHFR(DD)-Flt23k mRNA and protein levels in the retinas of OIR rats were quantified using qPCR and western blotting. DHFR(DD)-Flt23k gene expression was significantly increased in retinas from scAAV2-DHFR(DD)-Flt23k-injected rats compared with those from scAAV2-DHFR(DD)-mCherry-injected rats (**Figure 3f**). No statistically

significant difference (p=0.8410) in the DHFR(DD)-Flt23k mRNA level was found between scAAV2-DHFR(DD)-Flt23k-injected rats treated with TMP (118.5 ± 36.95-fold; n=3) and those not treated with TMP (132.7 ± 55.14-fold; n=3). DHFR(DD)-Flt23k proteins were detected only in retinas from scAAV2-DHFR(DD)-Flt23k/TMP-injected rats; no protein was found in retinas from scAAV2-mCherry/vehicle- or scAAV2-DHFR(DD)-Flt23k/vehicle-injected rats (**Figure 3g**). These results demonstrate that scAAV2 can effectively deliver DHFR(DD)-Flt23k to the retina in OIR rats and that subsequent administration of TMP is able to stabilize the expressed DHFR(DD)-Flt23k protein.

scAAV2-mediated gene delivery of DHFR(DD)-Flt23k reduces VEGF levels and attenuates retinal neovascularization in the OIR rat model.

The rat OIR model was applied to evaluate the therapeutic potential of drug-tunable DHFR(DD)-Flt23k gene therapy in retinal neovascularization. P7 pups were intravitreally injected with scAAV2-mCherry, scAAV2-Flt23k, scAAV2-DHFR(DD)-mCherry or scAAV2-DHFR(DD)-Flt23k. On P14 and P16, rats received intraperitoneal injections of TMP. Eyes were then harvested on P18 to evaluate VEGF expression and pathological blood vessel formation on the surface of the retina (retinal neovascularization; **Figures 4a and S4a**). Increased mRNA and protein expression of VEGF was observed in the retina of OIR rats on P18 (**Figure S4b and S4c**). Compared with eyes that received scAAV2-mCherry (VEGF: 39.9 ± 4.1 pg/mL; n=8), those intravitreally injected with scAAV2-Flt23k (VEGF: 28.5 ± 2.6 pg/mL, p<0.05; n=8) showed a significantly reduced level of VEGF in the retina (**Figure 4b**). Surprisingly, we found that VEGF expression was significantly reduced in retinas from scAAV2-DHFR(DD)-Flt23k/vehicle-injected rats (VEGF: 27.3 ± 1.5 pg/mL, p<0.05; n=8) and scAAV2-DHFR(DD)-Flt23k/TMP-injected rats (VEGF: 22.9 ± 1.4 pg/mL, p<0.01; n=8) compared with those from scAAV2-DHFR(DD)-mCherry/vehicle-injected rats (VEGF: 42.3 ± 4.8 pg/mL; n=8) or scAAV2-DHFR(DD)-mCherry/TMP-injected rats (VEGF: 37.8 ± 3.7 pg/mL; n=8) (**Figure 5b**). A slight reduction in the retinal VEGF level was found in scAAV2-DHFR(DD)-Flt23k/TMP-injected

8

rats compared to scAAV2-DHFR(DD)-Flt23k/vehicle-injected rats, but this difference did not reach statistical significance (p=0.0508) (**Figure 4b**). The results indicate that DHFR(DD)-Flt23k can reduce VEGF levels in the retina even without TMP administration.

We subsequently evaluated the therapeutic potential of the drug-tunable Flt23k gene delivery system in retinal neovascularization *in vivo*. Small tufts of vascular endothelial cells were observable at the edge of new blood vessel growth adjacent to avascular areas (**Figures 4c and S5**). Compared with intravitreal injection of scAAV2-mCherry (neovascular area: $3.23 \pm 0.25\%$ [95% confidence interval (CI): 2.68-3.78]; n=15), intravitreal injection of scAAV2-Flt23k significantly inhibited neovascularization (neovascular area: $1.57 \pm 0.14\%$ [95% CI: 1.28-1.86], p<0.001; n=20) (**Figure 4d**). In the drug-tunable system, a significant inhibition of retinal neovascularization was observed between scAAV2-DHFR(DD)-Flt23k-injected rats treated with TMP ($1.28 \pm 0.13\%$ [95% CI: 1.02-1.55], p<0.05; n=20) and those not treated with TMP ($1.95 \pm 0.12\%$ [95% CI: 1.69-2.20]; n=23) (**Figure 4d**). Similarly, there was a significant reduction in the neovascular area ($1.28 \pm 0.13\%$ [95% CI: 1.02-1.55], p<0.001; n = 20) in retinas from scAAV2-DHFR(DD)-Flt23k/TMP-injected rats compared with those from scAAV2-DHFR(DD)-mCherry/TMP-injected rats (neovascular area: $2.94 \pm 0.25\%$ [95% CI: 2.40-3.48]; n=17) (**Figure 4d**). We also found a reduction in the retinal neovascular area in scAAV2-DHFR(DD)-Flt23k/vehicle-injected rats (neovascular area: $1.95 \pm 0.12\%$ [95% CI: 1.69-2.20], p<0.01; n=23) compared with rats injected with scAAV2-DHFR(DD)-mCherry/vehicle (neovascular area: $2.49 \pm 0.23\%$ [95% CI: 2.00-2.98]; n=19) (**Figure 4d**). Moreover, no significant difference in the avascular area was observed among the 6 groups (**Figure 4e**). Together, our results demonstrate that gene delivery of DHFR(DD)-Flt23k by scAAV2 allows controlled suppression of retinal neovascularization in OIR rats via the administration of TMP.

Discussion

226   In the present study, we demonstrate that the DHFR(DD)-protein destabilizing system may be a

227   promising way to regulate the level of Flt23k in the retina for tailored suppression of retinal

228   neovascularization. Our *in vitro* studies showed that fusion of Flt23k to the N terminus of DHFR(DD)

229   allowed relatively good control of Flt23k expression with TMP. We showed that in a dose-dependent

230   manner, TMP increased the expression of Flt23k, which was functional with the capacity to attenuate

231   intracellular and extracellular VEGF levels in cells exposed to hypoxic conditions. Finally, intravitreal

232   gene delivery of DHFR(DD)-Flt23k by scAAV2 and subsequent administration of TMP provided

233   evidence for tunable attenuation of ischemia-induced retinal neovascularization in a rat model of OIR.

234   Rapid advances in gene therapy have brought this approach nearly to clinical use in

235   ophthalmology. Given that the eye is a particularly favorable organ for gene delivery, ocular use is

236   likely to be among the most successful applications of this technique. We provided proof-of-principle

237   evidence that intravitreal injection of scAAV2 under a ubiquitous cytomegalovirus (CMV) promoter

238   in OIR rats resulted in efficient and high-level transgene expression within a time frame relevant to

239   the treatment of retinal neovascularization. scAAV2 has been shown to exhibit better transduction

240   efficiency and faster initiation of gene expression in the retina than conventional single-stranded

241   AAVs[13,14]. However, the ubiquitous CMV promoter cannot be used to express anti-VEGF

242   therapeutic genes in specific cell types (i.e., Müller glial cells and photoreceptors) that are the primary

243   source of VEGF production in proliferative retinopathies. As such, it will be important to develop a

244   better delivery system with either a cell-specific promoter or an AAV variant that targets desired cell

245   types. Such refinements will lead to more effective therapies while reducing the potential for adverse

246   effects.

247   In this study, we show that using scAAV2 to deliver Flt23k can modify VEGF levels and

248   reduce retinal neovascularization in OIR rats. A similar therapeutic effect was also observed with

249   AAV-mediated gene delivery of Flt23k in a murine model of choroidal neovascularization[11].

250   However, high-level expression of an anti-VEGF protein such as Flt23k in the retina may have

251 unwanted consequences. Strategies are needed to regulate transgene expression through the

252 incorporation of trigger elements into the expression cassette, which are then modulated by an

253 exogenous drug[15] or endogenous molecules generated as part of the disease process[16]. Different

254 from those approaches, a protein-destabilizing system based on *E. coli* DHFR(DD) was used here. In

255 this system, the engineered DHFR(DD) is rapidly degraded along with any attached protein. A small-

256 molecule pharmacological chaperone (protein stabilizer) such as TMP, a common antibiotic, allows

257 newly synthesized DDs to be folded and stabilized at higher steady-state levels within cells, thus

258 protecting the attached therapeutic protein from degradation[17]. An appealing aspect of this strategy

259 to stabilize therapeutic proteins is that TMP, which is safe and able to cross the blood-retina barrier,

260 can be administered orally at a chosen time, such as during an exacerbation of retinal angiogenesis[9].

261 Oral or topical administration of TMP reliably prevents proteasomal destruction of DD-fused proteins

262 (delivered via an AAV) in the rodent retina without impacts on retinal function or structure[11,9].

263 Thus, TMP-mediated tunable gene therapy could meet the clinical requirement for a tailored and

264 sustained therapeutic intervention to treat retinal neovascularization.

265 Although promising in several regards, the DHFR(DD) destabilizing system requires further

266 refinement. Specifically, we observed that low protein levels of DHFR(DD)-Flt23k were present in

267 transfected cells not treated with TMP, suggesting that not all DHFR(DD)-fusion proteins were

268 degraded. Indeed, a significant reduction in the cytosolic VEGF level was seen in DHFR(DD)-Flt23k-

269 transfected cells and the retina of scAAV2-DHFR(DD)-Flt23k-injected eyes without the addition of

270 TMP. Additionally, Flt23k is a recombinant construct consisting of domain 2/3 of the VEGFR1

271 receptor coupled with a C-terminal ER-retention signal sequence (KDEL)[10]. The ER-retention

272 signal sequence allows newly formed fusion proteins to be retained in the ER[18], thus delaying their

273 degradation and leading to VEGF binding. However, newly formed fusion proteins may generate a

274 pull effect between the ER-retention signal and the protein-destabilizing signal of DHFR(DD)-Flt23k,

275 which may result in a delay in protein degradation, thereby increasing the amount of undegraded

protein in the cytosol. The undegraded or intermediate DHFR(DD)-Flt23k protein can potentially neutralize cytosolic VEGF and modulate the angiogenic response even without TMP stabilization. This might account for our observation that retinal neovascularization was reduced in scAAV2-DHFR(DD)-Flt23k-treated rats compared to those that received scAAV2-DHFR(DD)-mCherry. As OIR is a relatively acute model of retinal neovascularization with a low level of VEGF upregulation, a small increase in VEGF suppression can impact neovascularization. Thus, rats receiving scAAV2-DHFR(DD)-Flt23k could express low levels of undegraded or intermediate DHFR(DD)-Flt23k protein, which could neutralize retinal VEGF over time. A higher protein level of stabilized DHFR(DD)-Flt23k was observed upon TMP injection on P14 and P16 and led to more effective neutralization and thus a greater suppressive effect on retinal neovascularization. Therefore, our drug-tunable Flt23k gene therapy might be improved by removing the ER-retention signal sequence and adjusting the viral dose to reduce basal VEGF inhibition. Further studies in a clinically relevant model of chronic retinal neovascularization will further inform differences in the benefits of this tunable system.

A limitation of our work was that the safety of the drug-tunable Flt23k gene therapy in the retina was not evaluated in our proof-of-concept experiments. However, two recent studies have reported the safety profile of retinal Flt23k gene therapy and systemic TMP administration in mice. Zhang *et al*. reported that subretinal AAV-mediated gene delivery of Flt23k had no impact on retinal function or morphology for up to 6 months[11]. Datta *et al*. showed that there was no impact on the visual function or structure of the mouse retina after 3 months of TMP treatment[9]. Although these two studies have indicated that these strategies are safe in the retina, it will be important to assess the safety of both AAV-mediated Flt23k gene delivery and TMP administration before current research can be clinically translated. Another limitation of the present study was that the treatment was evaluated with a single dose of TMP (10 mg/kg) over a relatively short period of time in OIR rats. The TMP dose used in this study (10 mg/kg) was based on published reports[8,9] and is within the recommended dose for humans (10-15 mg/kg)[19]. As indicated by other reports and our *in vitro* data,

the dose of TMP impacts the expression of the stabilized DHFR(DD)-Flt23k protein. Therefore, the dose and frequency of TMP administration will need to be further optimized to match a drug-tunable Flt23k gene therapy system to the protracted time course of clinical disease processes.

Consistent with previous studies, this study showed that protein expression was dependent on the TMP dose. Although maximizing the TMP dose to achieve the optimal therapeutic effect is critical, the systemic administration of high-dose TMP may also have deleterious effects. Indeed, our *in vitro* study showed that a high dose of TMP could also inhibit VEGF mRNA expression (**Figure S1**). High doses of TMP can induce cell toxicity[20], thus modifying VEGF mRNA expression under hypoxia condition. Therefore, administration of high-dose TMP together with DHFR(DD)-Flt23k gene delivery may act synergistically to suppress VEGF at both the transcriptional level and the posttranslational level. In addition, prolonged oral TMP administration has been shown to disrupt the gut microbiome, which can impact the central nervous system[21] and in turn modify the progression of ocular diseases[22]. Thus, topical administration of TMP via eye drops may be a safer alternative. One study of the rodent retina demonstrated that topical administration of TMP could reliably and locally stabilize the expression of proteins fused to DHFR(DD) (delivered via an AAV)[9]. Moreover, to further mitigate systemic adverse events, a TMP-based nonantibiotic small molecule has been developed to control DHFR(DD)-fused proteins[23]. Therefore, a combination of nonantibiotic eye drops and tunable Flt23k gene therapy would be a safe and attractive approach for the treatment of retinal neovascularization.

In summary, our data suggest that the DHFR(DD)-protein destabilizing system is a promising way to regulate the level of Flt23k in the retina and provides the potential to tailor suppression of retinal neovascularization. Although further investigations are required to assess long-term safety and efficacy in clinically relevant models, we believe that this comprehensive strategy has the potential as a treatment strategy for retinal neovascularization and avoids the need for repeated intravitreal injections.

326

327

Materials and Methods

The sources of the materials and equipment used in this study are listed in **Table S1**.

Cell culture. HEK293A (catalog no. R70507; Life Technologies Australia, Mulgrave, VIC, Australia) and HEK293D (a gift from Dr. Ian Alexander at the Children's Medical Research Institute, University of Sydney, Australia) cells were cultured in Dulbecco's modified Eagle's medium (DMEM; catalog no. 11965092; Life Technologies Australia) supplemented with 10% fetal bovine serum (catalog no. F9423; Sigma-Aldrich, St. Louis, MO, USA), 50 U/mL penicillin-streptomycin (catalog no. 15070-063; Life Technologies Australia) and 2 mM glutamine (catalog no. 2503008; Life Technologies Australia). Cell lines were confirmed to be free of mycoplasma using the MycoAlert™ Mycoplasma Detection Kit (catalog no. LT07; Lonza, Walkersville, MD, USA) and cultured in a humidified 5% CO_2 atmosphere at 37 °C.

Transfection. Plasmid transfection was performed with Lipofectamine 2000 (catalog no. 11668019; Life Technologies Australia). In brief, HEK293A cells were plated in a 6-well plate on day 0 (2.5×10^5/well) and transfected with 750 ng of plasmid DNA using the protocol provided in the kit. After 24 hours of incubation, the transfection medium was replaced with fresh medium and treated with TMP (0, 2, 10, or 50 μM; catalog no. T7883; Sigma-Aldrich). Thereafter, cells were either exposed to hypoxia (GENbag anaer hypoxia bag, catalog no. 45534; bioMeriux, Marcy-l'Étoile, France) or kept in normoxia for 24 hours. Cell lysates and conditioned medium were then harvested for ELISA and qPCR.

349

AAV construction and virus production. EGFP, mCherry, Flt23k, DHFR(DD)-YFP, DHFR(DD)-mCherry, Flt23k-DHFR(DD) and DHFR(DD)-Flt23k complementary DNA (cDNA) sequences surrounded by AgeI/NotI cleavage sites were obtained by gene synthesis (GenScript, Piscataway, NJ, USA) and subcloned into the pHpa-trs-SK-EGFP plasmid (a gift from Dr. Douglas M. McCarty at the Center for Gene Therapy, Nationwide Children's Hospital, USA) by replacing the EGFP sequence. The Flt23k DNA sequence was kindly provided by Dr. Balamurali K Ambati at the Moran Eye Center (University of Utah, USA). The DHFR(DD) DNA sequence was based on pBMN-DHFR(DD)-YFP (a gift from Dr. Thomas Wandless at the Stanford University, USA; Addgene plasmid #29325). Recombinant scAAV2s were packaged as previously described[24]. Briefly, the scAAV2s were prepared by transfecting HEK293D cells with the targeted plasmids (pscAAV-mCherry, pscAAV-Flt23k, pscAAV-DHFR(DD)-YFP, pscAAV-DHFR(DD)-mCherry, pscAAV-DHFR(DD)-Flt23k or pHpa-trs-SK-EGFP), a helper plasmid (pXX6, kindly provided by the UNC Vector Core Facility, USA) and an AAV2 capsid plasmid (pXX2, kindly provided by the UNC Vector Core Facility, USA) using the calcium phosphate method. Viral vectors were purified using the AAVpro Purification Kit (catalog no. 6666; Clontech Laboratories, Mountain View, CA, USA), and titers were quantified by qPCR.

Western blot analysis. Cells or retinas were collected in 150 μL of Pierce RIPA buffer (catalog no. 89900; Life Technologies Australia) with a protease inhibitor cocktail (catalog no. 14692300; Roche Diagnostics, Basilea, Swiss). The lysates were homogenized using a sonicator for 5-10 seconds and then centrifuged at full speed for 15 minutes at 4 °C. The supernatants were collected and quantified using a Pierce™ BCA assay kit (catalog no. 23227; Life Technologies Australia). Proteins were denatured at 85 °C for 10 minutes, followed by separation on NuPAGE™ Novex™ 4-12% Bis-Tris Protein Gels (catalog no. NP0321BOX; Life Technologies Australia) using gel electrophoresis and transfer to polyvinylidene fluoride membranes (catalog no. IPVH00010; Immobilon-P; Merck Millipore, Burlington, MA, USA) using the XCell II™ Blot Module (Life Technologies Australia) at

375   30 volts for 1 hour. The membranes were then blocked with 5% skim milk in TBS-T (10 mM Tris,

376   150 mM NaCl, and 0.05% Tween-20) at room temperature for 1 hour and incubated with a mouse anti-

377   VEGFR1 antibody (Flt-1/EWC) (1:500 dilution; catalog no. ab9540; Abcam, Cambridge, UK)

378   overnight at 4 °C or with a mouse anti-GAPDH antibody (clone 6C5, 1:500 dilution; catalog no.

379   MAB374; Merck Millipore) or mouse anti-Actin antibody (clone C4, 1:5000 dilution; catalog no.

380   MAB1501; Merck Millipore) at room temperature for 1 hour. The membranes were washed and further

381   incubated with a goat anti-mouse IgG HRP-conjugated secondary antibody (1:4000 dilution; catalog

382   no. 12-349; Merck Millipore) at room temperature for 1 hour. The membranes were then developed

383   using the Amersham ECL Prime Western Blotting Detection Kit (catalog no. RPN2235; GE

384   Healthcare Australia, Parramatta, NSW, Australia).

385

386   **ELISA.** The VEGF protein level was detected in HEK293A cell lysates, conditioned media and rat

387   retinal tissue lysates using ELISA. For cell and tissue lysates, samples were prepared in Pierce RIPA

388   buffer. Lysates and conditioned media were analyzed using human or rat VEGF ELISA kits (catalog

389   no. DY293B and RRV00; R&D Systems, Inc., Minneapolis, MN, USA) per the manufacturer's

390   instructions, and results were read at a 450-nm wavelength using a CLARIOstar microplate reader

391   (BMG LABTECH, Ortenberg, Germany).

392

393   **qPCR.** Total RNA was extracted and purified from cells or retinas using TRIzol Reagent (catalog no.

394   15596026; Life Technologies Australia) according to the manufacturer's instructions. cDNA synthesis

395   from total RNA was achieved using a high-capacity RT kit (catalog no. 4368814; Life Technologies

396   Australia). Two nanograms of cDNA were used for real-time PCR using an ABI QuantStudio3 device

397   (Applied Biosystems, Foster City, CA, USA) and TaqMan Fast Master mix (catalog no. 4444557; Life

398   Technologies Australia) with the TaqMan assay probes for *VEGFA* (Hs00900054_m1). Human

399   *HPRT1* (Hs99999909_m1) was used as the reference gene. Transcript levels were calculated using the

400   ΔΔCt method, as previously described by Livak[25].

401

402   **Animals.** Female Sprague-Dawley rats were supplied by the Cambridge Farm Facility of the

403   University of Tasmania and housed in standard cages with free access to food and water in a

404   temperature-controlled environment under a 12-h light (50 lux illumination)/12-h dark (< 10 lux

405   illumination) cycle to minimize possible light-induced eye damage. All animal experiments described

406   adhered to the guidelines of the Association for Research in Vision and Ophthalmology Statement for

407   the Use of Animals in Ophthalmic and Vision Research and were approved by the Animal Ethics

408   Committee of the University of Tasmania, Australia (ethics approval number A0017598).

409

410   **Rat model of OIR and vessel quantification.** We employed a modified rat OIR protocol based on a

411   previous study[26]. Briefly, newborn Sprague-Dawley rats and their nursing mothers were housed in

412   a commercially available chamber (A-Chamber; BioSpherix, Parish, NY, USA) within 12 hours of

413   birth (P0) and exposed to daily cycles of 80% O_2 for 21 hours and room air for 3 hours from P0 to P14.

414   The pups were then returned to room air until P18. An oxygen controller (ProOx 110; BioSpherix)

415   was used to monitor and control the oxygen level in the humidified chamber. The rats were sacrificed

416   on P18, and their retinas were dissected and stained with 5 g/mL Alexa Fluor™ 488-conjugated

417   isolectin B4 (isolectin GS-IB4 from *Griffonia simplicifolia*; catalog no. I21411; Life Technologies

418   Australia). The sizes of the neovascularization and vaso-obliteration areas in the rat retinas were

419   quantified with Adobe Photoshop (CC 2017.1.1) by two blinded assessors (JC and GSL). If the

420   isolectin GS-IB4-labeled retinal vascular area was < 20% of the total retinal area, the sample was

421   excluded from the study.

422

423 **Intravitreal injection.** Intravitreal injections of AAVs were performed under a surgical microscope.

424 In brief, after making a guide track through the conjunctiva and sclera at the superior temporal

425 hemisphere behind the limbus using a 30-gauge needle, a hand-pulled glass micropipette connected to

426 a 10-µL Hamilton syringe (Bio-Strategy, Broadmeadows, VIC, Australia) was inserted into the vitreal

427 cavity. A total of 1 µL of AAVs (2-2.5x10^9 viral genomes) was injected into an eye of OIR rats on P7,

428 and an equal amount of saline was injected into the contralateral eye of the same animal. A total of

429 192 neonatal rats (from 20 litters) were used in our *in vivo* study. Animals were randomly allocated

430 into the following groups: scAAV2-EGFP (n=5), scAAV2-mCherry (n=29), scAAV2-Flt23k (n=30),

431 scAAV2-DHFR(DD)-YFP (n=10), scAAV2-DHFR(DD)-mCherry (n=52), and scAAV2-DHFR(DD)-

432 Flt23k (n=66). Any issues arising from the injection, including large backflow upon removal of the

433 needle and the presence of hemorrhaging anywhere on the eye, resulted in exclusion from the study.

434

435 **TMP administration.** OIR rats were intraperitoneally injected with a TMP lactate salt (catalog no.

436 T0667; Sigma-Aldrich) or vehicle on P14 and P16. TMP was freshly dissolved in nanopure water and

437 diluted to a concentration of 30 mg/mL. Rats were given 100 µL of this solution, which equates to 3

438 mg of TMP/rat/dose.

439

440 **Immunofluorescence analysis.** Rat pups were euthanized on P18. Eyeballs were removed and fixed

441 in a 4% formaldehyde solution in PBS for 1 hour at room temperature. The cornea and lens were

442 removed, and the globes were incubated with 18% sucrose until the eyeball sank to the bottom of the

443 container at room temperature. The eyes were then placed in 30% sucrose overnight. Samples were

444 embedded in optimal cutting temperature compound (catalog no. IA018; ProSciTech, Kirwan, QLD,

445 Australia) and stored at -80 °C. Serial cryosections (20-µm thickness) were obtained and stored at -20

446 °C. The sections were rinsed in three washes of PBS and then underwent immunofluorescence labeling

447 with NucBlue™ Live Cell Stain ReadyProbes Reagent (catalog no. R3760S; Life Technologies

448 Australia) for 20 minutes and an anti-GFAP antibody (1:500 dilution; catalog no. G3893; Merck

449 Millipore) for 1 hour. The sections were washed and mounted with Dako fluorescent mounting

450 medium (catalog no. s3020; DAKO, Carpinteria, CA, USA). Images were digitized using a

451 fluorescence microscope (Zeiss Axio Imager Microscope; Carl-Zeiss-Strasse, Oberkochen, Germany)

452 equipped with a charge-coupled digital camera (Axiocam MRm, Zeiss) and image acquisition software

453 (ZEN2, Zeiss). The entire retina was photographed using appropriate filters to capture the fluorescence

454 emission spectra of mCherry (610 nm), EGFP/isolectin B4-FITC (509 nm), and NucBlue (460 nm),

455 and separate images were merged to form a complete image of the retinal section. The fluorescence of

456 the EGFP-positive area in the total retina was quantified with ImageJ.

457

458 **Statistical analysis.** Statistical analysis was performed using GraphPad Prism 7 for all experimental

459 data. Measurement data are presented as the mean ± standard error of the mean (SEM). Comparisons

460 among multiple groups were analyzed by two-tailed Student's *t*-tests, one-way or two-way ANOVA

461 followed by Tukey's multiple comparisons. Values were determined to be significant when the p value

462 was less than 0.05.

463

475

476 **Competing Interests**

477 The authors have declared that no competing interest exists.

478

479 **Data Availability**

480 All datasets generated for this study are included in the article/supplementary materials.

481

482 **Author contributions**

483 Conceptualization- J.C., G-S.L. Methodology- J.C., F-L.L., J.Y.K.L., G-S.L. Formal Analysis- J.C.,

484 F-L.L., G-S.L. Investigation- J.C., F-L.L., J.Y.K.L., L.T., Y-F.C., J-H.W., F.L., V.H.Y.W. Resources-

485 G.J.D., H-H.S., B.V.B., L.L., A.W.H., J.Z., G-S.L. Data Curation- J.C., G-S.L. Writing (Original

486 Draft)- J.C., G-S.L. Writing (Review & Editing)- J.Y.K.L., J-H.W., F-L.L., L.L., G.J.D., V.H.Y.W.,

487 B.V.B., J.Z. Visualization- J.C., G-S.L. Supervision- J.Z., G-S.L. Project Administration- J.C., G-S.L.

488 Funding Acquisition- J.Z., G-S.L.

Figure Captions

Graphical Abstract. Schematic diagram of the tunable **system utilizing the DHFR(DD)-Flt23k approach to reduce VEGF secretion**. **(a)** The schematic shows normal VEGF secretion. **(b)** Without the ligand TMP, the DHFR(DD)-Flt23k protein is destabilized and degraded by the proteasome. **(c)** In the presence of the ligand TMP, DHFR(DD)-Flt23k is stabilized and sequestered in the ER, thereby conditionally inhibiting VEGF. Green lines indicate the intracellular and extracellular distributions of VEGF. Blue lines indicate proteasomal degradation of the DHFR(DD)-Flt23k protein. Orange lines indicate the uptake of cell-permeable TMP. TMP, trimethoprim; VEGF, vascular endothelial growth factor; ER, endoplasmic reticulum.

Figure 1. Characterization of DHFR(DD)-Flt23k gene transfer *in vitro*. **(a)** The schematic illustrates conditional protein stabilization by the ligand TMP. The DHFR(DD)-fused Flt23k protein is an unstable cytosolic protein that is rapidly degraded by the proteasome unless protected by the specific cell-permeable ligand TMP. **(b)** The schematic shows plasmid constructs. **(c and d)** Two days after transfection, the expression of Flt23k or DHFR(DD) fused with Flt23k in HEK293A cells in the presence of 0 or 10 µM TMP was confirmed by western blotting. The graph shows the quantification of protein expression. Two-tailed Student's t-tests were performed to determine the significance of differences (***$p < 0.001$, *$p < 0.05$). **(e and f)** The DHFR(DD)-Flt23k level in HEK293A cells was increased by TMP in a dose-dependent manner (0-50 µM). The graph shows the quantification of protein expression. Two-tailed Student's t-tests were performed to determine the significance of differences (**$p<0.01$; #$p<0.05$ compared to DHFR(DD)-Flt23k with 0 µM TMP). All data are presented as the mean ± SEM. Corresponding uncropped images of western blots are shown in **Figure S6**. CMV, cytomegalovirus; mCH, mCherry; EGFP, enhanced green fluorescent protein; YFP, yellow fluorescent protein; TMP, trimethoprim.

Figure 2. Stabilization of DHFR(DD)-Flt23k inhibits intracellular and extracellular VEGF. Cells were transfected and treated with different doses of TMP (0, 2, 10, or 50 µM), followed by treatment with hypoxia for 24 hours. Histograms show that compared to DHFR(DD)-YFP or DHFR(DD)-Flt23k, stabilized DHFR(DD)-Flt23k inhibits intracellular **(a)** and extracellular **(b)** VEGF expression, as detected by ELISA. One-way ANOVA followed by Tukey's multiple-comparisons test was performed to determine the significance of differences (***$p<0.001$, **$p<0.01$, *$p<0.05$). All data are presented as the mean ± SEM. mCH, mCherry; YFP, yellow fluorescent protein; TMP, trimethoprim.

Figure 3. scAAV2-mediated gene transduction following intravitreal injection into the retina of OIR rats. Representative images of retinal flat-mount sections **(a)** and cross-sections **(b and c)** from OIR rats (P18) 11 days after scAAV2-EGFP intravitreal injection. Intact retinas were confirmed with NucBlue™ (blue) staining. **(a)** Retinal flat mounts showing EGFP expression distribution (green). Scale bars: 1 mm. **(b)** Distribution and colocalization of EGFP (green) and GFAP staining (retinal glial cell marker, red) in retinal cross-sections. Scale bars: 500 µm. **(c)** High-magnification view of a retinal cross-section. Transduction of retinal cells is evident by the presence of EGFP-positive cells in the outer nuclear layer (arrows) and inner segments. Scale bars: 100 µm. **(d)** Schematic diagram of the rat OIR model protocol to illustrate the timing of viral vector injection and intraperitoneal TMP injection. **(e)** Retinal flat-mount section showing TMP-mediated YFP protein stabilization in an OIR rat. Scale bars: 1 mm (left panels) and 70 µm (right panels). **(f)** DHFR(DD)-Flt23k mRNA expression levels in retinas injected with scAAV2-DHFR(DD)-mCherry or scAAV2-DHFR(DD)-Flt23k with or without TMP, as quantified using qPCR (n=3). Two-tailed Student's t-tests were performed to evaluate differences between groups. All data are presented as the mean ± SEM. **(g)** Retinal DHFR(DD)-Flt23k protein levels determined using western blotting, each with three replicates. Corresponding uncropped images of western blots are shown in **Figure S6**. OIR, oxygen-induced retinopathy; EGFP, enhanced

green fluorescent protein; GFAP, glial fibrillary acidic protein; mCH, mCherry; YFP, yellow fluorescent protein; TMP, trimethoprim; GCL, ganglion cell layer; INL, inner nuclear layer; ONL, outer nuclear layer.

Figure 4. Effects of intravitreal scAAV2 injection on retinal neovascularization in the rat OIR model. (**a**) Schematic of the rat OIR model protocol to illustrate the timing of viral vector injection and intraperitoneal TMP injection. Neonatal rats were exposed to daily cycles of 80% oxygen for 21 hours and room air for 3 hours from P0 to P14 and received an intraperitoneal injection of 3 mg of TMP on P14 and P16. On P14, the animals were returned to room air until P18. scAAV2-mCherry, scAAV2-Flt23k, scAAV2-DHFR(DD)-mCherry, or scAAV2-DHFR(DD)-Flt23k was injected on P7. (**b**) Rat retinal VEGF levels quantified using ELISA analysis of 8 retinas (3 littermates). One-way ANOVA followed by Tukey's multiple comparisons test was performed to determine the significance of differences (**$p<0.01$, *$p<0.05$). (**c**) A typical cluster of vascular structures represented as "neovasculature" on a flat-mounted retina harvested on P18 after intravitreal injections on P7 and stained with isolectin B4. Retinal neovascularization is highlighted in white, and insets show the selected areas at high magnification. Scale bars: 250 μm. Corresponding uncropped images of retinas are shown in **Figure S5**. (**d**) Retinal neovascular area quantified from 15 to 23 retinas. One-way ANOVA followed by Tukey's multiple-comparisons test was performed to compare groups (***$p<0.001$, **$p<0.01$, *$p<0.05$). (**e**) Retinal avascular area quantification. Data are presented as the mean ± SEM from 11 to 22 retinas. No significant difference was observed in the avascular area. All data are presented as the mean ± SEM. OIR, oxygen-induced retinopathy; mCH, mCherry; TMP, trimethoprim.

562 **Table S1. Key Resources**

REAGENT or RESOURCE	SOURCE	IDENTIFIER
Antibodies		
Mouse anti-VEGF receptor 1 antibody (Flt-1/EWC)	Abcam	Cat# ab9540
Mouse anti-GFAP antibody	Millipore	Cat# G3893
Mouse anti-GAPDH (clone 6C5) antibody	Chemicon	Cat# MAB374
Mouse anti-Actin (clone C4) antibody	Millipore	Cat# MAB1501
Goat anti-mouse IgG HRP-conjugated secondary antibody	Millipore	Cat# 12-349
Isolectin GS-IB4 From Griffonia simplicifolia, Alexa Fluor™ 488 Conjugate	Life Technologies Australia	Cat# I21411
NucBlue™ Live Cell Stain ReadyProbes Reagent	Life Technologies Australia	Cat# R3760S
Plasmid DNA		
pHpa-trs-SK-EGFP	Kindly provided by Dr Douglas M. McCarty, Center for Gene Therapy, Nationwide Children's Hospital, USA	n/a
pXX2	Kindly provided by UNC Vector Core Facility, USA	n/a
pXX6	Kindly provided by UNC Vector Core Facility, USA	n/a
pscAAV-mCherry	The plasmid was generated by Liu Lab from this study	Vector backbone: pHpa-trs-SK

pscAAV-Flt23k	The plasmid was generated by Liu Lab from this study	Vector backbone: pHpa-trs-SK
pscAAV-DHFR(DD)-YFP	The plasmid was generated by Liu Lab from this study	Vector backbone: pHpa-trs-SK
pscAAV-DHFR(DD)-mCherry	The plasmid was generated by Liu Lab from this study	Vector backbone: pHpa-trs-SK
pscAAV-DHFR(DD)-Flt23k	The plasmid was generated by Liu Lab from this study	Vector backbone: pHpa-trs-SK
pscAAV-Flt23k-DHFR(DD)	The plasmid was generated by Liu Lab from this study	Vector backbone: pHpa-trs-SK
Chemicals		
Glutamine	Life Technologies Australia	Cat# 2503008
Penicillin-streptomycin	Life Technologies Australia	Cat# 15070063
Trimethoprim	Sigma-Aldrich	Cat# T7883
Trimethoprim lactate salt	Sigma-Aldrich	Cat# T0667
Critical Commercial Assays		
MycoAlert™ Mycoplasma Detection Kit	Lonza, Walkersville	Cat# LT07
AAVpro Purification Kit	Clontech Laboratories	Cat# 6666
Pierce™ BCA assay kit	Life Technologies Australia	Cat# 23227
Amersham ECL Prime Western Blotting Detection Kit	GE Healthcare Australia	Cat# RPN2235

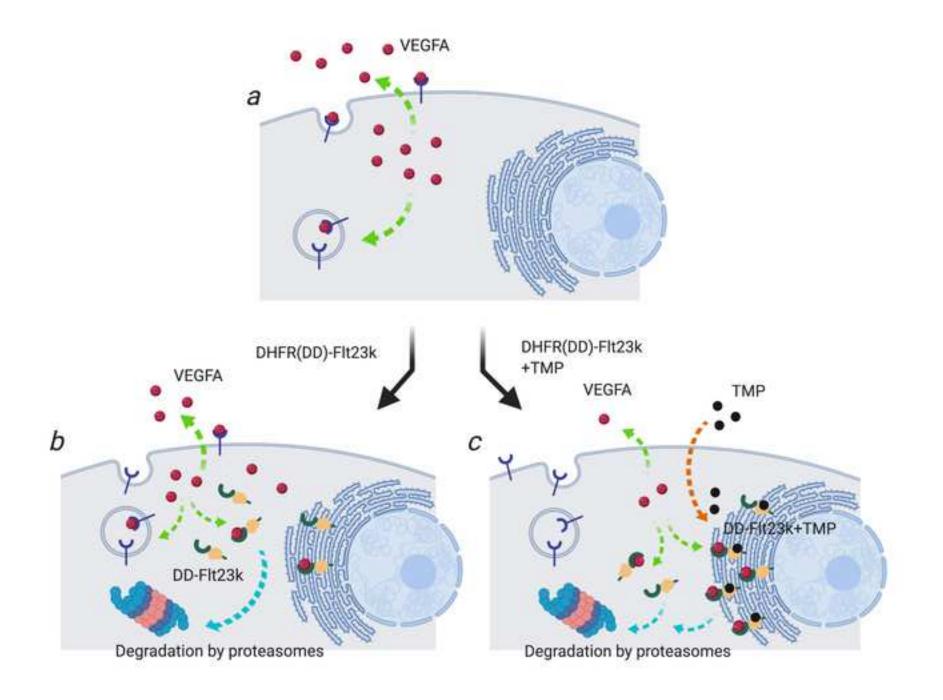|		
DuoSet® Ancillary Reagent Kit 2	R&D Systems	Cat# DY008
Duoset® human ELISA VEGF Kit	R&D Systems	Cat# DY293B-05
Rat VEGF Quantikine ELISA Kit	R&D Systems	Cat# RRV00
High capacity cDNA reverse transcription Kit	Life Technologies Australia	Cat# 4368814
TaqMan Fast Master mix	Life Technologies Australia	Cat# 4444557
Experimental Models: Cell Lines		
Human embryonic kidney 293A	Life Technologies Australia	Cat# R70507
Human embryonic kidney 293D	Kindly provided by Professor Ian Alexander at the Children's Medical Research Institute, Australia	n/a
Experimental Models: Organisms/Strains		
Sprague-Dawley rat	Cambridge Farm Facility in University of Tasmania, Hobart, Australia	AEC: 004/16
Equipment		
CLARIOstar microplate reader	BMG LABTECH, Ortenberg	n/a
QuantStudio3	Applied Biosystems	n/a
Oxygen controller, ProOx 110	BioSpherix	n/a

Hamilton syringe	Bio-Strategy	n/a
Zeiss Axio Imager Microscope	Carl-Zeiss-Strasse, Oberkochen, Germany	n/a
qPCR Probes		
Human *VEGFA* TaqMan probe sequences: N/A	Applied Biosystems	Hs00900054_m1
Human *HPRT1* TaqMan probe sequences: N/A	Applied Biosystems	Hs99999909_m1
Software and Algorithms		
ImageJ version 1.48	Schneider et al., 2012	https://imagej.nih.gov/ij
Prism 7	GraphPad Software	n/a
Adobe Photoshop (CC 2017.1.1)	Connor et al., 2009	Adobe
Other		
Dulbecco's modified Eagle's medium	Life Technologies Australia	Cat# 11965092
Fetal bovine serum	Sigma-Aldrich	Cat# F9423
Opti-MEM I reduced serum medium	Life Technologies Australia	Cat# 31985088
Lipofectamine 2000	Life Technologies Australia	Cat# 11668019
Hypoxia bag	BioMeriux	Cat# 45534

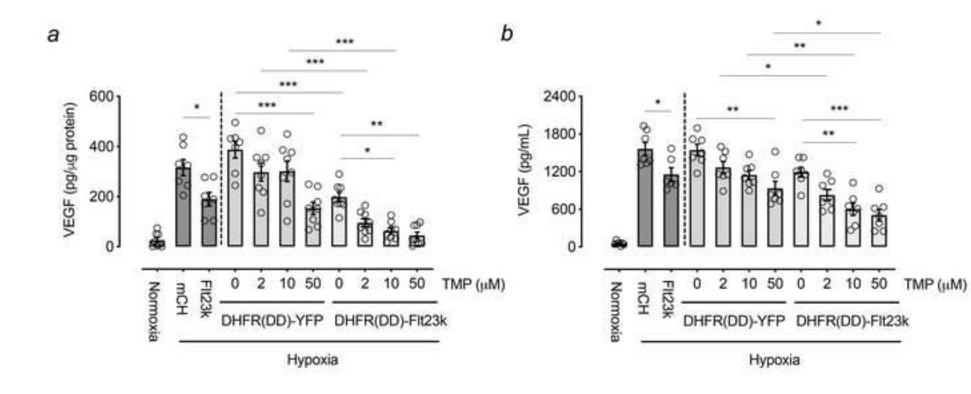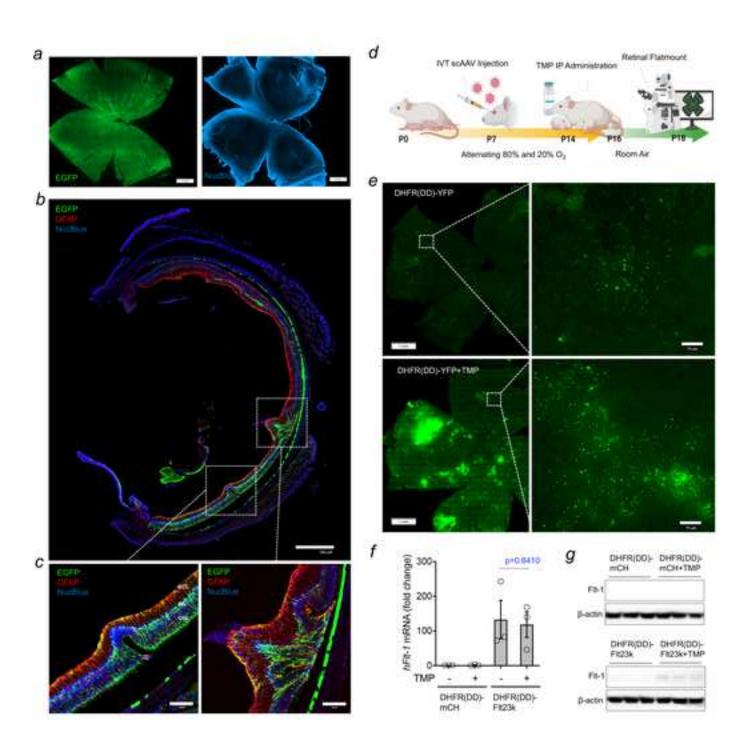|		
Anaerotic indicator	BioMeriux	Cat# 96118
Pierce RIPA buffer	Life Technologies Australia	Cat# 89900
Protease Inhibitor Cocktail	Roche Diagnostics	Cat# 14692300
NuPAGE™ Novex™ 4-12% Bis-Tris Protein Gels	Life Technologies Australia	Cat# NP0321BOX
Polyvinylidene fluoride membranes	Millipore	Cat# IPVH00010
XCell II™ Blot Module	Life Technologies Australia	Cat# 11965118
Trizol Reagent	Life Technologies Australia	Cat# 15596026
Optimal cutting temperature compound	ProSciTech	Cat# IA018
Dako Fluorescent mounting medium	DAKO	Cat# S3020

563
564

References

565 **References**

566 1. Sun Y, Smith LEH (2018) Retinal Vasculature in Development and Diseases. Annu Rev Vis Sci
567 4:101-122

568 2. Wells JA, Glassman AR, Ayala AR, Jampol LM, Aiello LP, Antoszyk AN, Arnold-Bush B, Baker
569 CW, Bressler NM, Browning DJ, Elman MJ, Ferris FL, Friedman SM, Melia M, Pieramici DJ, Sun
570 JK, Beck RW (2015) Aflibercept, bevacizumab, or ranibizumab for diabetic macular edema. N Engl J
571 Med 372 (13):1193-1203

572 3. Mehta H, Tufail A, Daien V, Lee AY, Nguyen V, Ozturk M, Barthelmes D, Gillies MC (2018) Real-
573 world outcomes in patients with neovascular age-related macular degeneration treated with intravitreal
574 vascular endothelial growth factor inhibitors. Prog Retin Eye Res 65:127-146.
575 doi:10.1016/j.preteyeres.2017.12.002

576 4. Avery RL, Gordon GM (2016) Systemic Safety of Prolonged Monthly Anti-Vascular Endothelial
577 Growth Factor Therapy for Diabetic Macular Edema: A Systematic Review and Meta-analysis. JAMA
578 Ophthalmol 134 (1):21-29. doi:10.1001/jamaophthalmol.2015.4070

579 5. Rakoczy EP, Lai CM, Magno AL, Wikstrom ME, French MA, Pierce CM, Schwartz SD,
580 Blumenkranz MS, Chalberg TW, Degli-Esposti MA, Constable IJ (2015) Gene therapy with
581 recombinant adeno-associated vectors for neovascular age-related macular degeneration: 1 year
582 follow-up of a phase 1 randomised clinical trial. Lancet 386 (10011):2395-2403. doi:10.1016/s0140-
583 6736(15)00345-1

584 6. Heier JS, Kherani S, Desai S, Dugel P, Kaushal S, Cheng SH, Delacono C, Purvis A, Richards S,
585 Le-Halpere A, Connelly J, Wadsworth SC, Varona R, Buggage R, Scaria A, Campochiaro PA (2017)
586 Intravitreous injection of AAV2-sFLT01 in patients with advanced neovascular age-related macular
587 degeneration: a phase 1, open-label trial. Lancet 390 (10089):50-61. doi:10.1016/s0140-
588 6736(17)30979-0

589 7. Luo L, Zhang X, Hirano Y, Tyagi P, Barabás P, Uehara H, Miya TR, Singh N, Archer B, Qazi Y,
590 Jackman K, Das SK, Olsen T, Chennamaneni SR, Stagg BC, Ahmed F, Emerson L, Zygmunt K,
591 Whitaker R, Mamalis C, Huang W, Gao G, Srinivas SP, Krizaj D, Baffi J, Ambati J, Kompella UB,
592 Ambati BK (2013) Targeted intraceptor nanoparticle therapy reduces angiogenesis and fibrosis in
593 primate and murine macular degeneration. ACS Nano 7 (4):3264-3275. doi:10.1021/nn305958y

594 8. Santiago CP, Keuthan CJ, Boye SL, Boye SE, Imam AA, Ash JD (2018) A Drug-Tunable Gene
595 Therapy for Broad-Spectrum Protection against Retinal Degeneration. Mol Ther 26 (10):2407-2417

596 9. Datta S, Renwick M, Chau VQ, Zhang F, Nettesheim ER, Lipinski DM, Hulleman JD (2018) A
597 Destabilizing Domain Allows for Fast, Noninvasive, Conditional Control of Protein Abundance in the
598 Mouse Eye - Implications for Ocular Gene Therapy. Invest Ophthalmol Vis Sci 59 (12):4909-4920

599 10. Singh N, Amin S, Richter E, Rashid S, Scoglietti V, Jani PD, Wang J, Kaur R, Ambati J, Dong Z,
600 Ambati BK (2005) Flt-1 intraceptors inhibit hypoxia-induced VEGF expression in vitro and corneal
601 neovascularization in vivo. Invest Ophthalmol Vis Sci 46 (5):1647-1652. doi:10.1167/iovs.04-1172

602 11. Zhang X, Das SK, Passi SF, Uehara H, Bohner A, Chen M, Tiem M, Archer B, Ambati BK (2015)
603 AAV2 delivery of Flt23k intraceptors inhibits murine choroidal neovascularization. Mol Ther 23
604 (2):226-234

605 12. Egeler EL, Urner LM, Rakhit R, Liu CW, Wandless TJ (2011) Ligand-switchable substrates for a
606 ubiquitin-proteasome system. J Biol Chem 286 (36):31328-31336. doi:10.1074/jbc.M111.264101

607 13. Yokoi K, Kachi S, Zhang HS, Gregory PD, Spratt SK, Samulski RJ, Campochiaro PA (2007)
608 Ocular gene transfer with self-complementary AAV vectors. Invest Ophthalmol Vis Sci 48 (7):3324-
609 3328. doi:10.1167/iovs.06-1306

610 14. McCarty DM (2008) Self-complementary AAV vectors; advances and applications. Mol Ther 16
611 (10):1648-1656. doi:10.1038/mt.2008.171

612 15. St-Onge L, Furth PA, Gruss P (1996) Temporal control of the Cre recombinase in transgenic mice
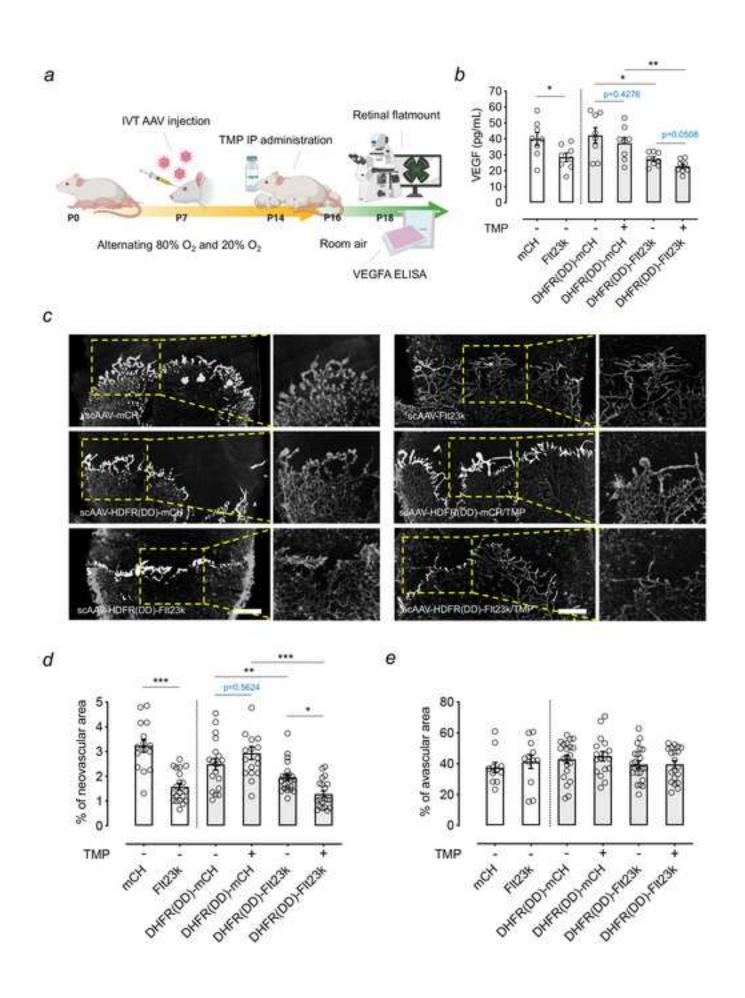613 by a tetracycline responsive promoter. Nucleic Acids Res 24 (19):3875-3877

614   16. Prentice HM, Biswal MR, Dorey CK, Blanks JC (2011) Hypoxia-regulated retinal glial cell-
615   specific promoter for potential gene therapy in disease. Invest Ophthalmol Vis Sci 52 (12):8562-8570
616   17. Iwamoto M, Bjorklund T, Lundberg C, Kirik D, Wandless TJ (2010) A general chemical method
617   to regulate protein stability in the mammalian central nervous system. Chem Biol 17 (9):981-988
618   18. Munro S, Pelham HR (1987) A C-terminal signal prevents secretion of luminal ER proteins. Cell
619   48 (5):899-907. doi:10.1016/0092-8674(87)90086-9
620   19.   Sulfamethoxazole   /   Trimethoprim   Dosage   (2019)
621   https://www.drugs.com/dosage/sulfamethoxazole-trimethoprim.html.
622   20. Güzel Bayülken D, Bostancıoğlu RB, Koparal AT, Ayaz Tüylü B, Dağ A, Benkli K (2018)
623   Assessment of in vitro cytotoxic and genotoxic activities of some trimethoprim conjugates.
624   Cytotechnology 70 (3):1051-1059. doi:10.1007/s10616-018-0187-7
625   21. Carabotti M, Scirocco A, Maselli MA, Severi C (2015) The gut-brain axis: interactions between
626   enteric microbiota, central and enteric nervous systems. Ann Gastroenterol 28 (2):203-209
627   22. Rowan S, Jiang S, Korem T, Szymanski J, Chang ML, Szelog J, Cassalman C, Dasuri K, McGuire
628   C, Nagai R, Du XL, Brownlee M, Rabbani N, Thornalley PJ, Baleja JD, Deik AA, Pierce KA, Scott
629   JM, Clish CB, Smith DE, Weinberger A, Avnit-Sagi T, Lotan-Pompan M, Segal E, Taylor A (2017)
630   Involvement of a gut-retina axis in protection against dietary glycemia-induced age-related macular
631   degeneration. Proc Natl Acad Sci U S A 114 (22):E4472-e4481. doi:10.1073/pnas.1702302114
632   23. Peng H, Chau VQ, Phetsang W, Sebastian RM, Stone MRL, Datta S, Renwick M, Tamer YT,
633   Toprak E, Koh AY, Blaskovich MAT, Hulleman JD (2019) Non-antibiotic Small-Molecule Regulation
634   of DHFR-Based Destabilizing Domains In Vivo. Mol Ther Methods Clin Dev 15:27-39
635   24. Xiao X, Li J, Samulski RJ (1998) Production of high-titer recombinant adeno-associated virus
636   vectors in the absence of helper adenovirus. J Virol 72 (3):2224-2232
637   25. Livak KJ, Schmittgen TD (2001) Analysis of relative gene expression data using real-time
638   quantitative PCR and the 2(-Delta Delta C(T)) Method. Methods 25 (4):402-408.
639   doi:10.1006/meth.2001.1262
640   26. Penn JS, Tolman BL, Henry MM (1994) Oxygen-induced retinopathy in the rat: relationship of
641   retinal nonperfusion to subsequent neovascularization. Invest Ophthalmol Vis Sci 35 (9):3429-3435
642

Figure 1

Click here to access/download;Figure;Figure 1.tif

Figure 2

Click here to access/download;Figure;Figure 2.tif ⬇

Figure 3

Click here to access/download;Figure;Figure 3.tif ⬇

Figure 4

Click here to access/download;Figure;Figure 4.tif

Click here to access/download
Supplementary Material
Flt23k gene therapy _supplemental
materials_R2_26082020.docx